Origin of Unexpectedly Simple Oscillatory Responses in the Excited-State Dynamics of Disordered Molecular Aggregates

Origin of unexpectedly simple oscillatory responses in the excited-state dynamics of disordered molecular aggregates

Maxim F. Gelin,*,† Raffaele Borrelli,‡ and Wolfgang Domcke†

†*Department of Chemistry, Technische Universität München, D-85747 Garching, Germany*

‡*DISAFA, Università di Torino, I-10095 Grugliasco, Italy*

E-mail: gelin@ch.tum.de

Abstract

Unraveling the many facets of coherent and incoherent exciton motion in an ensemble of chromophores is an inherently complex quantum mechanical problem that has triggered a vivid debate on the role of quantum effects in molecular materials and biophysical systems. Here the dynamics of a statistical ensemble of molecular aggregates consisting of identical chromophores is investigated within a new theoretical framework. Taking account of intrinsic properties of the system, the Hamiltonian of the aggregate is partitioned into two mutually commuting vibrational and vibronic operators. This representation paves the way for an analysis which reveals the role of the static disorder in ensembles of aggregates. Using analytical methods, it is demonstrated that after a critical time $\tau_D \simeq 2\pi/\sigma$ (σ being the dispersion of the disorder) any dynamic variable of the aggregate exhibits purely vibrational dynamics. This result is illustrated by exact numerical calculations of the time-dependent site populations of the aggregate. These findings may be useful for the interpretation of recent femtosecond spectroscopic experiments on molecular aggregates.

Photoinduced dynamical phenomena in molecular aggregates are topics at the forefront of contemporary research which extends from the uncovering of mechanisms of photosynthetic light harvesting in living organisms to the design of efficient optoelectronic materials and devices.[1–3] The basic paradigm for the understanding of photophysical properties of molecular aggregates is the notion of the exciton, a quasiparticle generated by optical excitation of electronically coupled chemically identical chromophores. In the simplest picture, the chromophores are treated as electronic two-level systems. In reality, they are polyatomic molecules with a large number of nuclear degrees of freedom. Upon aggregation, these molecules form complexes revealing highly nontrivial photoinduced vibronic dynamics.

In 2007, it was suggested that long-lived coherent electronic dynamics in the excitonic states of antenna complexes at room temperature may have functional significance for light harvesting.[4] In the following years this paradigm became widely accepted in the photosynthetic community and beyond.[5] At the beginning of the 2010s, this paradigm underwent modification owing to a growing body of evidence that exciton-vibrational coupling is instrumental for the explanation of the observed excited-state coherent responses.[6] Recently, the significance of electronic coherent effects for photosynthesis at room temperature was questioned.[7] The latest experimental data[8,9] as well as numerical simulations[10–12] indicate that the oscillatory responses in spectroscopic signals may predominantly reveal vibrational wave-packet dynamics in the electronic ground state of the aggregate.

These findings indicate that the elucidation of the mechanistic role of exciton-vibrational couplings in the photophysics of molecular aggregates is of fundamental significance. This topic has been the subject of numerous theoretical studies which, due to the complexity of the problem, were mostly based on numerical simulations of specific systems at various levels of accuracy.[13–16] In this communication, we present analytical results and results of accurate numerical simulations which explain the emergence of purely vibrational signatures in the excited-state dynamics of molecular aggregates in the presence of static disorder.

First, exploiting the structure of the excitonic Hamiltonian, we demonstrate that this

Hamiltonian can be written as the sum of two commuting operators, one of which generates pure vibrational dynamics. Second, we show that static disorder causes a "melting" of exciton-vibrational dynamics into pure vibrational dynamics. We provide evidence that the expectation value of any dynamical variable in the *excited* states of a molecular aggregate exhibits purely vibrational dynamics after a critical time $\tau_D \simeq 2\pi/\sigma$, where σ is the dispersion of the static disorder.

Consider a molecular aggregate consisting of N_e identical chromophores placed in a dissipative environment (solvent). Each chromophore is approximated as an electronic two-level system with N_v vibrational intramolecular and intermolecular modes. The Hamiltonian of this aggregate can be represented as a sum of the excitonic Hamiltonian H_e, vibrational Hamiltonian H_v, and their coupling H_{ev}:[13,14]

$$H = H_e + H_v + H_{ev}, \tag{1}$$

$$H_e = \sum_{k=1}^{N_e} \varepsilon_k B_k^\dagger B_k + \sum_{k \neq k'}^{N_e} J_{kk'} B_k^\dagger B_{k'}, \tag{2}$$

$$H_v = \sum_{k=1}^{N_e} \sum_{\alpha=1}^{N_v} \frac{\Omega_\alpha}{2} \left(P_{k\alpha}^2 + X_{k\alpha}^2 \right), \tag{3}$$

$$H_{ev} = \sum_{k=1}^{N_e} \sum_{\alpha=1}^{N_v} \Omega_\alpha \kappa_\alpha B_k^\dagger B_k X_{k\alpha}. \tag{4}$$

Here, $B_k^\dagger$ and B_k are exciton creation and annihilation operators at site k obeying the Pauli commutation rules $[B_k, B_{k'}^\dagger] = \delta_{kk'}(1 - 2B_k^\dagger B_{k'})$, ε_k are the electronic site energies, and $J_{kk'}$ $(k \neq k')$ are the inter-site electronic couplings; $X_{k\alpha}$, $P_{k\alpha}$ and Ω_α denote the dimensionless positions, dimensionless momenta, and frequencies of the harmonic mode α of chromophore k, and the parameters κ_α control the strength of the intra-site electron-vibrational coupling. Since the chromophores are identical, the Ω_α and κ_α are k-independent. The Hamiltonian (1) commutes with the exciton number operator $\hat{N}$ and therefore conserves the number of

excitations:

$$[H, \hat{N}] = 0, \quad \hat{N} \equiv \sum_{k=1}^{N_e} B_k^\dagger B_k. \tag{5}$$

In order to partially disentangle the coupled exciton-vibrational dynamics of the aggregate, we introduce N_v totally symmetric vibrational coordinates and conjugated momenta

$$q_\alpha = \frac{1}{\sqrt{N_e}} \sum_{k=1}^{N_e} X_{k\alpha}, \quad p_\alpha = \frac{1}{\sqrt{N_e}} \sum_{k=1}^{N_e} P_{k\alpha} \tag{6}$$

and $(N_e - 1) \times N_v$ internal vibrational coordinates $s_{k\alpha}$ and momenta $p_{k\alpha}$ (cf. Refs.[17,18]). As detailed in the Supplementary Material, this transformation of vibrational coordinates results in the expression

$$H = H_q + H_s. \tag{7}$$

Here

$$H_q = \sum_{\alpha=1}^{N_v} \frac{\Omega_\alpha}{2} \left(p_\alpha^2 + q_\alpha^2 + 2\kappa_\alpha q_\alpha \frac{\hat{N}}{\sqrt{N_e}} \right). \tag{8}$$

The explicit form of H_s, which depends on $s_{k\alpha}$, $p_{k\alpha}$ and B_k, is given in the Supplementary Material. In the special case of a dimer ($N_e = 2$) with two vibrational modes ($N_v = 2$) the partitioning (7) is well known in the literature.[10,19,20]

It can be readily verified that

$$[H_q, H_s] = 0. \tag{9}$$

Since the number of excitons is a constant of motion ($\hat{N} = N$), the Hamiltonian H_q represents N_v uncoupled oscillators with displacements $\kappa_\alpha N/\sqrt{N_e}$. H_s, on the other hand, describes the excitonic system coupled to the internal vibrational modes $s_{k\alpha}$. The dynamics in variables q_α is therefore separable from the dynamics in variables $s_{k\alpha}$.

Let us now evaluate the expectation value of a dynamical variable A

$$\langle A(t) \rangle = \mathrm{Tr}\left\{ \rho(t) A \right\}, \quad \rho(t) = e^{-iHt/\hbar} \rho(0) e^{iHt/\hbar}, \tag{10}$$

$\rho(0)$ being the initial density matrix. We formally introduce the eigenstate representations: $H_q\,|q\rangle = E_q\,|q\rangle$, $H_s\,|s\rangle = E_s\,|s\rangle$, and the corresponding vibrational transition frequencies

$$\omega_{qq'} = (E_q - E_{q'})/\hbar \tag{11}$$

and vibronic transition frequencies

$$\omega_{ss'} = (E_s - E_{s'})/\hbar. \tag{12}$$

Since H_q describes a set of N_v uncoupled shifted harmonic oscillators with frequencies Ω_α, its eigenfunctions $|q\rangle$ and eigenvalues E_q are known analytically. After changing to the eigenstate representation, Eq. (10) becomes

$$\langle A(t)\rangle = \sum_{q,q',s,s'} V_{qsq's'} e^{-i\omega_{qq'}t} e^{-i\omega_{ss'}t} \tag{13}$$

where $V_{qs,q's'} = \rho_{qs,q's'}(0) A_{q's',qs}$.

In reality, the aggregates are usually embedded in a polymer matrix or protein scaffold which produces static disorder in site energies ε_k and couplings $J_{kk'}$ (hereafter, these parameters are collectively denoted as y_j, $j = 1, 2, ..., \mathcal{K}$), while inhomogeneities in the vibrational parameters Ω_α and κ_α are likely much smaller and can be neglected. The macroscopic ensemble of aggregates is thus a realization of a large number of microscopic systems with the parameters

$$y_j = \bar{y}_j + z_j, \tag{14}$$

where $\bar{y}_j$ are mean values and z_j are random numbers with a certain distribution $g(\boldsymbol{z})$. The latter is typically given by a product of Gaussians with zero mean and variances (dispersions) σ_j, $j = 1, 2, ..., \mathcal{K}$. Hence the ensemble average of the expectation value of the dynamical

variable A is given by

$$\overline{\langle A(t)\rangle} = \int_{-\infty}^{\infty} d\boldsymbol{y}\, g(\boldsymbol{y}-\bar{\boldsymbol{y}})\mathrm{Tr}\left\{\rho(\boldsymbol{y},t)A\right\} \tag{15}$$

where $\rho(\boldsymbol{y},t)$ is given by Eq. (10) with $H \to H(\boldsymbol{y})$. The matrix elements $V_{qs,q's'}(\boldsymbol{y})$ and vibronic transition frequencies $\omega_{ss'}(\boldsymbol{y})$ also become $\boldsymbol{y}$-dependent, while the vibrational transition frequencies $\omega_{qq'}$ are $\boldsymbol{y}$-independent.

If $|\boldsymbol{\sigma}| \ll |\bar{\boldsymbol{y}}|$, then $\overline{\langle A(t)\rangle} \approx \mathrm{Tr}\left\{\rho(\bar{\boldsymbol{y}},t)A\right\}$. For pigment-protein complexes, however, $|\boldsymbol{\sigma}| \sim |\bar{\boldsymbol{y}}|$.[3] In this case, the effect of static disorder is nontrivial, but the averaging in Eq. (15) can be evaluated asymptotically, for $t \to \infty$, by using the stationary phase method. The detailed treatment and discussion, as well as the explicit expressions are given in the Supplementary Material. Here we present the final result. Let

$$\tau_D \simeq 2\pi/\sigma \tag{16}$$

be a characteristic time at which the asymptotic description becomes valid ($\sigma \approx \min \sigma_j$). Then for $t > \tau_D$ the expectation value of the dynamical variable exhibits purely vibrational oscillations and can be represented as

$$\overline{\langle A(t)\rangle} \approx \frac{a}{t^d} + b + \sum_{\alpha=1}^{N_v}\sum_{m=1}^{M}\left(\frac{a_{\alpha m}}{t^{d_{\alpha m}}} + b_{\alpha m}\right)\cos(m\Omega_\alpha t - \varphi_{\alpha m}). \tag{17}$$

Here the parameters a, b, d and $a_{\alpha m}$, $b_{\alpha m}$, $\varphi_{\alpha m}$, d_α can, in principle, be expressed in terms of $V_{qs,q's'}(\boldsymbol{y})$, $g(\boldsymbol{y})$ and $\omega_{ss'}(\boldsymbol{y})$, but their explicit evaluation is very tedious. Fortunately, this is not necessary. For practical use, Eq. (17) can merely be considered as an *Ansatz* for fitting $\overline{\langle A(t)\rangle}$ (*vide infra*). The Ω_α in Eq. (17) are the fundamental vibrational frequencies which are unaffected by static disorder, and the summation over m accounts for vibrational overtones. The term b yields the stationary contribution ($q = q'$, $s = s'$ in Eq. (10)). The terms $\sim b_{\alpha m}$ are generated by the vibrational Hamiltonian H_q ($q \neq q'$, $s = s'$ in Eq. (10)) or by vibrational modes which accidentally are decoupled from the excitonic degrees of freedom.

The algebraically decaying terms $\sim a$ and $\sim a_{\alpha m}$ originate from the averaging over static disorder. The crucial role of static disorder is thus to melt the time evolution governed by the vibronic frequencies $\omega_{ss'}(\boldsymbol{y})$ into the algebraically-decaying oscillatory contributions governed by multiples of the vibrational frequencies Ω_α. For $t \to \infty$, these algebraic contributions vanish and, if $b_{\alpha m} \neq 0$, $\overline{\langle A(t)\rangle}$ exhibits long-lived vibrational beatings.

To illustrate the validity and significance of the analytical results of Eq. (17), we performed numerical simulations of the time evolution of the population of site $k = 1$,

$$P_1(t) = \mathrm{Tr}\left\{\rho(t)|1\rangle\langle 1|\right\}, \quad \rho(0) = |1\rangle\langle 1|\rho_B. \tag{18}$$

Here $|1\rangle = B_1^\dagger|0\rangle$ describes an excitation on site 1, and $\rho_B = Z_B^{-1}\exp\{-H_v/(k_BT)\}$ is the vibrational Boltzmann distribution in the electronic ground state of the aggregate (Z_B is the partition function, k_B is the Boltzmann constant, and T is the temperature). $P_1(t)$ is an observable which as such is not measurable, but is of broad interest in theoretical studies of the nonequilibrium dynamics of excitonic systems.[15,16] Note that the time evolution of $P_1(t)$ is determined solely by the Hamiltonian H_s, since H_q commutes with $|1\rangle\langle 1|$.

The numerical simulations of $P_1(t)$ are performed by employing the Thermo-Field-Dynamics Tensor-Train method[21–24] which allows a numerically accurate evaluation of $P_1(t)$ at finite temperature (in the present case, $T = 300$ K). $\overline{P}_1(t)$ is obtained by the averaging of individual populations $P_1(t)$ over $\mathcal{N}_z$ realizations of $\boldsymbol{z}$.

The short-time evolution of $P_1(t)$ can be cast in the form

$$P_1(t) = \exp\{-(t/\tau_Z)^2\} + O(t^3), \tag{19}$$

where τ_Z is the so-called Zeno time.[25] For the Hamiltonian of Eq. (1), it can be evaluated analytically with the result

$$\tau_Z^{-2} = \sum_{k=1}^{N_e} J_{1k}^2. \tag{20}$$

Hence the short-time evolution is independent of the nuclear degrees of freedom and is exclusively determined by the excitonic couplings. For $t > \tau_D$, on the other hand, $\overline{P}_1(t)$ should be reproduced by Eq. (17). We found *a posteriori* that the overtones of the fundamental vibrational frequencies do not contribute to the time evolution of $P_1(t)$. We thus set $M = 1$, drop the subscripts m in Eq. (17), and treat a, b and a_α, b_α, φ_α as fitting parameters.

In model I, we consider a linear chain of $N_e = 7$ sites with identical site energies and nearest-neighbor couplings $J_{k,k+1} = 80$ cm^{-1}. Each site has a single vibrational mode with frequency $\Omega_1 = 200$ cm^{-1} (corresponding to a vibrational period $\tau_1 = 2\pi/\Omega_1 = 167$ fs), and an electron-vibrational coupling parameter $\kappa_1 = 100$ cm^{-1}. Static disorder in ε_k and $J_{k,k+1}$ is described by Eq. (14) in which z_j are $\mathcal{K} = 13$ uncorrelated Gaussian variables with variance $\sigma_j = \sigma = 100$ cm^{-1}. $\overline{P}_1(t)$ evaluated with $\mathcal{N}_z = 100$ is found to be numerically converged.

The results of the simulations are displayed in Fig. 1. The green line shows the $P_1(t)$ obtained by Eq. (19) with the Zeno time $\tau_Z = 66$ fs evaluated according to Eq. (20). The black line shows the numerically converged population $\overline{P}_1(t)$, while the blue line depicts $\overline{P}_1(t)$ averaged over just $\mathcal{N}_z = 5$ realizations of z_j. The red line shows the least square fit of $\overline{P}(t)$ by Eq. (17). It provides an *a posteriori* estimate of τ_D which can be defined as the shortest time at which Eq. (17) becomes accurate. The matching of the black, blue, and green curves for $t < \tau_Z$ reveals that the short-time dynamics is purely electronic and is independent of static disorder. According to Eq. (16), the characteristic time is $\tau_D = 334$ fs, which is close to the *a posteriori* estimate of $\tau_D = 420$ fs (beginning of the red curve).

In the interval $[\tau_Z, \tau_D]$, static disorder affects $\overline{P}_1(t)$ only marginally, hence the blue ($\mathcal{N}_z = 5$) and black ($\mathcal{N}_z = 100$) curves have similar shapes. For $t > \tau_D$, the blue curve shows partially irregular oscillations, while the black curve exhibits regular vibrational oscillations with the period τ_1. The agreement between the numerically exact $\overline{P}_1(t)$ (black) and fit by Eq. (17) (red) is almost perfect. It should be stressed that neither the blue curve nor any individual $P_1(t)$ simulated for a specific realization of $\boldsymbol{z}$ can be adequately fitted by Eq. (17). The latter reproduces the average population $\overline{P}_1(t)$ only.

Model II mimics the Fenna–Matthews–Olson (FMO) complex. It describes 7 identical chromophores ($N_e = 7$), each of which possesses two vibrational modes ($N_v = 2$): $\Omega_1 = 200$ cm^{-1} ($\tau_1 = 2\pi/\Omega_1 = 167$ fs) and $\Omega_2 = 160$ cm^{-1} ($\tau_2 = 2\pi/\Omega_2 = 208$ fs). These are the modes which were recently detected experimentally.[8,9] The electron-vibrational couplings are $\kappa_1 = 0.289$ and $\kappa_2 = 0.175$. The values of ε_k and $J_{kk'}$ are the same as in Ref.[22] Static disorder in ε_k and $J_{kk'}$ is accounted for by $\mathcal{K} = 29$ uncorrelated Gaussian variables z_j with variance $\sigma_j = \sigma = 100$ cm^{-1}.[3] $\overline{P}(t)$ evaluated for $\mathcal{N}_z = 500$ is numerically converged. Frequently, it is sufficient to account for static disorder in site energies only.[3,26] This case is considered in the Supplementary Material.

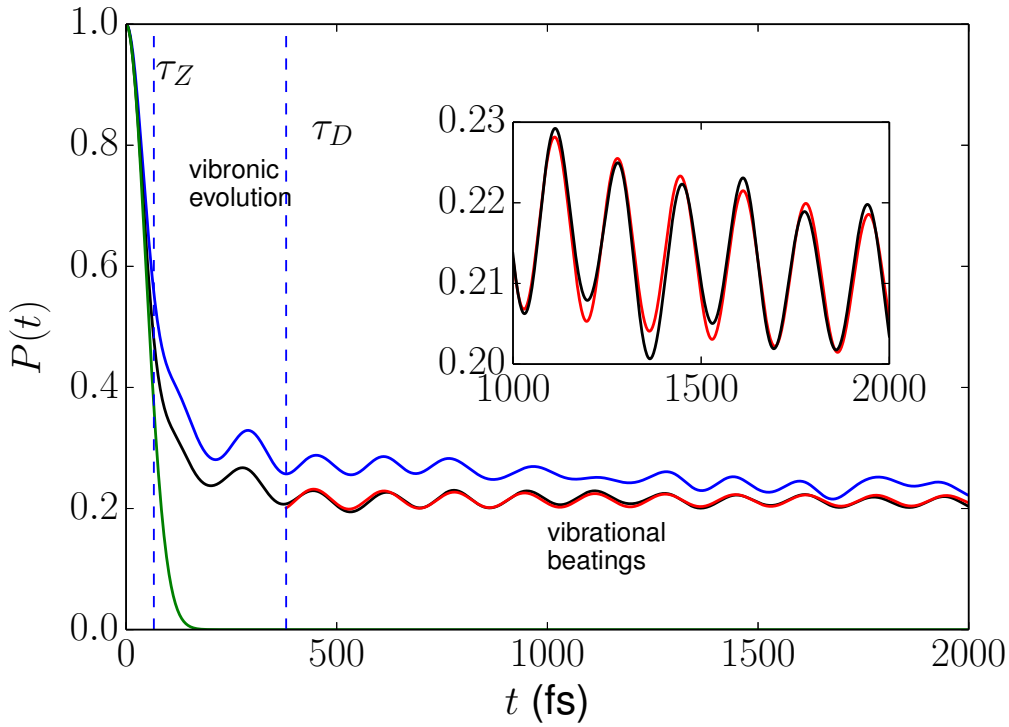

Figure 1: $P_1(t)$ for model I and $T = 300$ K. Black: Numerical evaluation for $\mathcal{N}_z = 100$. Blue: Numerical evaluation for $\mathcal{N}_z = 5$. Red: Fit via Eq. (17) with the parameters $a = 1.46$, $b = 0.21$, $a_1 = -7.16$, $b_1 = 0$, $\varphi_1 = 1.17$ and $d = d_1 = 0.5$. The inset shows the exact (black) and fitted (red) curves on an enlarged scale. Green: Eq. (19).

Fig. 2 provides an illustration of how individual realizations of static disorder affect the population dynamics. From bottom to top, it shows $P_1(t)$ for 9 individual realizations of

z_j. The uppermost graph (black) depicts the fully converged $\overline{P}_1(t)$ for $\mathcal{N}_z = 500$. The $P_1(t)$ obtained for 9 realizations of z_j differ from each other by the periods, phases, and amplitudes of the oscillations. Hence the average population $\overline{P}_1(t)$ is the result of the superposition of a large number of different oscillatory contributions.

Fig. 3 shows the numerically exact average population $\overline{P}_1(t)$ (black) in comparison with the short-time approximation by Eq. (20) with the Zeno time $\tau_Z = 53$ fs (green) and the least square fit via Eq. (17) (red). The critical time τ_D is *a posteriori* estimated to be ~ 500 fs. In the time interval $[\tau_Z, \tau_D]$, the evolution of $\overline{P}_1(t)$ is characterized by a strong mixture of the excitonic and vibrational degrees of freedom. For $t > \tau_D$, $\overline{P}_1(t)$ exhibits oscillations revealing the vibrational frequencies Ω_1 and Ω_2. In view of the complexity of the time evolution of $\overline{P}_1(t)$, the agreement between the exact simulation (black) and the fit (red) is quite impressive. The exact $\overline{P}_1(t)$ (black line in Fig. 3) exhibits a revival around $t \sim 1300$ fs. This effect is caused by the accidental commensurability of the vibrational frequencies: $4\Omega_1 = 5\Omega_2$. The vibrational beatings thus fully rephase at $5\tau_1 = 4\tau_2 \approx 830$ fs. The revival occurs ~ 830 fs after the asymptotic description starts to be valid, e.g. at $t \approx \tau_D + 830 \approx 1300$ fs, and is fairly well reproduced by the fit.

In summary, we have developed a generic picture of the time evolution of expectation values of dynamical variables in aggregates consisting of identical chromophores in the presence of static disorder. For $t < \tau_Z$ (τ_Z being the Zeno time) the time evolution is purely electronic. For $\tau_Z \leq t \leq \tau_D$ (τ_D being the critical time determined by the dispersion of the disorder) the time evolution is vibronic. For $t > \tau_D$ the observables exhibit purely vibrational behavior (cf. Ref.[27]).

The results of the present work may have profound implications for the interpretation of spectroscopic responses of chromophore aggregates. For example, the beatings with a period around ~ 200 fs detected in the recent experiments on FMO[8,9] may reveal vibrational dynamics not only due to the wave packet motion in the electronic ground state (ground state bleach contribution), but also owing to the disorder-induced melting of vibronic frequencies

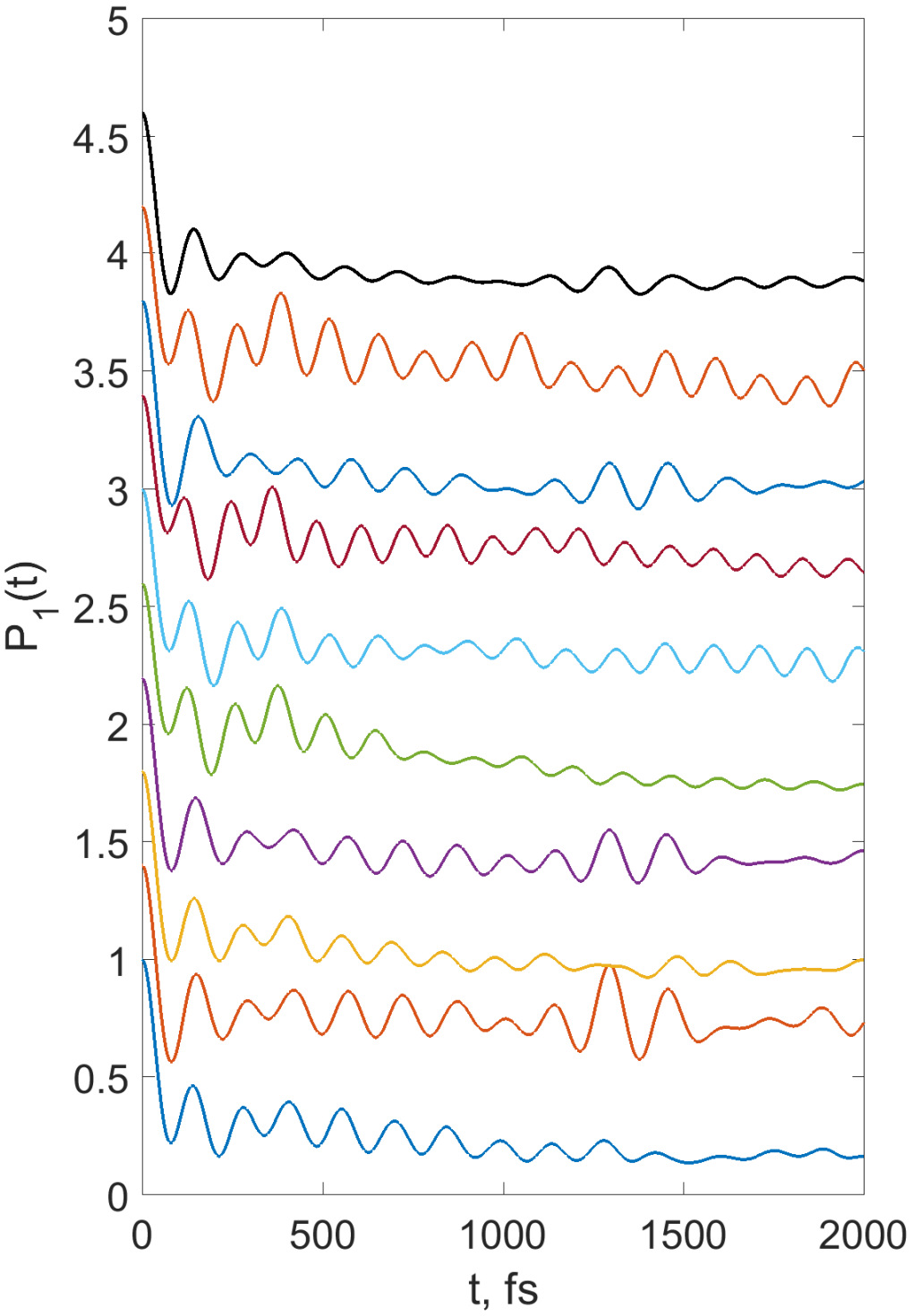

Figure 2: $P_1(t)$ for model II and $T = 300$ K. Colored curves: $P_1(t)$ for 9 realizations of z_j. Uppermost graph (black): converged $\overline{P}_1(t)$ evaluated for $\mathcal{N}_z = 500$. For clarity, the populations are vertically displaced from each other by 0.4.

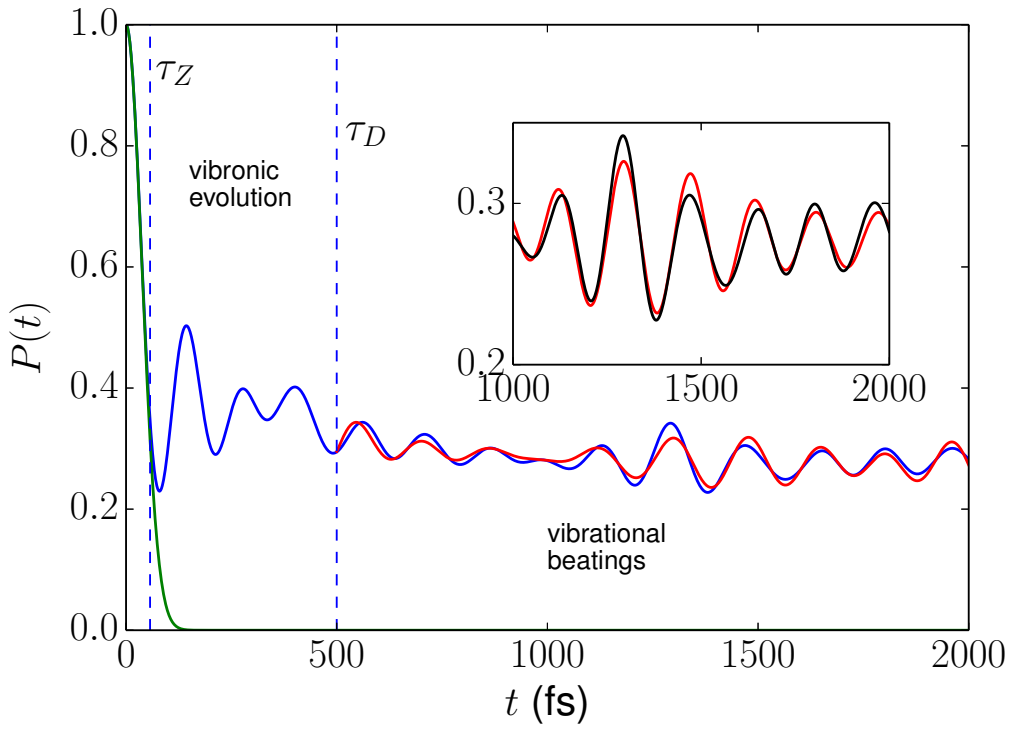

Figure 3: $P_1(t)$ for model II and $T = 300$ K. Black: Numerical evaluation for $\mathcal{N}_z = 500$. Red: Fit via Eq. (17) with the parameters $a = 1.81$, $b = 0.23$, $a_1 = 3.69$, $b_1 = -0.12$, $\varphi_1 = 1.99$, $a_2 = -1.01$, $b_2 = 0.04$, $\varphi_2 = 1.05$ and $d = d_1 = d_2 = 0.5$. The inset shows the exact (black) and fitted (red) curves on an enlarged scale. Green: Eq. (19).

into vibrational frequencies in the excited electronic state (stimulated emission contribution). More generally, any pump-probe or photon-echo signal as a function of population time will always be dominated by vibrational oscillations at $t > t_D$.

Acknowledgement

M. F. G. and W. D. acknowledge support by the Deutsche Forschungsgemeinschaft through a research grant and through the DFG Cluster of Excellence Munich-Centre for Advanced Photonics (http://www.munich-photonics.de). R. B. acknowledges the CINECA awards TFDTT-HP10CWGIMW and TFQD-HP10CU8XMP under the ISCRA initiative for the availability of high performance computing resources and support as well as the University of Torino for the award BORR-RILO-17-01. We are grateful to Luca Celardo and Jianshu Cao for useful discussions.

Supporting Information Available

The following files are available free of charge.

- Supplement.pdf: Contains the explicit partitioning of the full Hamiltonian, the evaluation of $\overline{\langle A(t)\rangle}$ by the stationary phase method, and the analysis of $\overline{P}_1(t)$ for FMO in the case of static disorder in site energies.

References

(1) Brixner, T.; Hildner, R.; Köhler, J.; Lambert, C.; Würthner, F. *Advanced Energy Materials* **2017**, *7*, 1700236.

(2) Spano, F. C. *Acc. Chem. Res.* **2010**, *43*, 429–439.

(3) Mirkovic, T.; Ostroumov, E. E.; Anna, J. M.; Grondelle, R. v.; Govindjee,; Scholes, G. D. *Chem. Rev.* **2017**, *117*, 249.

(4) Engel, G. S.; Calhoun, T. R.; Read, E. L.; Ahn, T.-K.; Mančal, T.; Cheng, Y.-C.; Blankenship, R. E.; Fleming, G. R. *Nature* **2007**, *446*, 782.

(5) Scholes, G. D. et al. *Nature* **2017**, *543*, 647.

(6) Malý, P.; Somsen, O. J. G.; Novoderezhkin, V. I.; Mančal, T.; van Grondelle, R. *ChemPhysChem* **2016**, *17*, 1356.

(7) Duan, H.-G.; Prokhorenko, V. I.; Cogdell, R. J.; Ashraf, K.; Stevens, A. L.; Thorwart, M.; Miller, R. J. D. *Proc. Natl. Acad. Sci. USA* **2017**, *114*, 8493.

(8) Maiuri, M.; Ostroumov, E. E.; Saer, R. G.; Blankenship, R. E.; Scholes, G. D. *Nature Chemistry* **2018**, *10*, 177–183.

(9) Thyrhaug, E.; Tempelaar, R.; Alcocer, M. J. P.; Žídek, K.; Bína, D.; Knoester, J.; Jansen, T. L. C.; Zigmantas, D. *Nature Chemistry* **2018**, *10*, 780.

(10) Tiwari, V.; Peters, W. K.; Jonas, D. M. *Proc. Natl. Acad. Sci. USA* **2013**, *110*, 1203.

(11) Tempelaar, R.; Jansen, T. L. C.; Knoester, J. *J. Phys. Chem. B* **2014**, *118*, 12865.

(12) Fujihashi, Y.; Fleming, G. R.; Ishizaki, A. *J. Chem. Phys.* **2015**, *142*, 212403.

(13) Chernyak, V.; Mukamel, S. *J. Chem. Phys.* **1996**, *105*, 4565.

(14) Mukamel, S.; Abramavicius, D. *Chem. Rev.* **2004**, *104*, 2073–2098.

(15) Schröter, M.; Ivanov, S. D.; Schulze, J.; Polyutov, S. P.; Yan, Y.; Pullerits, T.; Kühn, O. *Physics Reports* **2015**, *567*, 1–78.

(16) Jang, S. J.; Mennucci, B. *Rev. Mod. Phys.* **2018**, *90*, 035003.

(17) Gelin, M. F.; Egorova, D.; Domcke, W. *Phys. Rev. E* **2011**, *84*, 041139.

(18) Spano, F. C.; Yamagata, H. *J. Phys. Chem. B* **2011**, *115*, 5133.

(19) Fulton, R. L.; Gouterman, M. *J. Chem. Phys.* **1964**, *41*, 2280.

(20) Gelin, M. F.; Sharp, L. Z.; Egorova, D.; Domcke, W. *J. Chem. Phys.* **2012**, *136*, 034507.

(21) Borrelli, R.; Gelin, M. F. *J. Chem. Phys.* **2016**, *145*, 224101.

(22) Borrelli, R.; Gelin, M. F. *Scientific Reports* **2017**, *7*, 9127.

(23) Gelin, M. F.; Borrelli, R. *Annalen der Physik* **2017**, *529*, 1700200.

(24) Borrelli, R. *Chem. Phys.* **2018**, *515*, 236–241.

(25) Facchi, P.; Pascazio, S. *Fortschritte der Physik* **2001**, *49*, 941.

(26) Renger, T.; El-Amine Madjet, M.; Schmidt am Busch, M.; Adolphs, J.; Müh, F. *Photosynth. Res.* **2013**, *116*, 367.

(27) Kreisbeck, C.; Kramer, T. *J. Phys. Chem. Lett.* **2012**, *3*, 2828–2833.